Probing the Richness Mass Proxy with Magneticum Simulation Galaxy Clusters

Bachelor thesis at the Faculty of Physics
Ludwig-Maximilians-University Munich

Submitted by
Maximilian Kai Kühn
born in Baden-Baden

Supervised by
Dr. Klaus Dolag

Munich, 31th of July 2017

Richness als Massen - Skalierungsrelation von Galaxienhaufen in der Magneticum Simulation

Bachelorarbeit der Fakultät für Physik
der
Ludwig-Maximilians-Universität München

vorgelegt von
Maximilian Kai Kühn
geboren in Baden-Baden

betreut von
Dr. Klaus Dolag

München, den 31.07.2017

Contents

Chapter 1

Introduction: Why study galaxy clusters?

The hierarchical model of structure formation in the universe assumes matter to collapse in small regions first, which accumulate themselves and form bigger and bigger structures. This results in so called self similarity, which can indeed be observed. In the primordial universe however, it was not possible for baryonic matter to retain bound states and therefore collapse. The universe was extremely hot and dense, causing high energy photons to destroy electro magnetic bonds. Dark matter, on the other hand, interacts only gravitationally, thus being able to maintain and grow density fluctuations. The pattern of dark matter overdensities was determined by quantum fluctuations that in a time of extremely fast expansion of space (called inflation) froze out, because the space expanded much faster than light speed, giving matter no opportunity to reach thermal equilibrium. These overdensities are the seeds for the filament structure, which later forms from gravitational collapse as we know from dark matter simulations. Since the universe cooled while expanding, the number density of high energy photons became small enough to enable barionic structure growth. These structures formed in the already existing potential wells of dark matter, because the principle of maximum entropy wants everything to be in the lowest possible energy state. Galaxy clusters are the largest astronomical structures in the universe that had time to collapse and virialize. Standing between astrophysics and cosmology, they play a very special role. They allow us to measure several properties. Sunyaev Zeldovic effect, X-ray and optical observations, gravitational lensing and velocity dispersion being few of them. On the other hand the resulting number density and mass distributions are sensitive to the underlying cosmological parameters, giving the opportunity to check the cosmological model.

Dynamics in galaxy clusters happens in time scales that are not observable in our lifetime, which is no surprise, knowing their size. Nevertheless, it is possible to see time development, because of the constance of light speed. Hence, looking further away is equivalent to looking in the past. However, observing at high redshifts is limited by the sensitivity of telescopes. This makes numerical simulations inevitable for a deeper understanding of structure formation and the physical processes behind it. Numerical simulations included gradually more and more physical processes. Beginning with dark matter only simulations over hydrodynamics to feedback processes. However it is important to be careful, that if the physical processes are not self consistently reproduced, the deeper mechanism is still hidden. Physical properties in simulations are mostly calculated differently than in observations, since velocities and positions can be measured directly and in three dimensions.

Therefore, it is important to know the approach of observers for a better comparison. A big difference is projection for example. Observers can only measure two dimensionally, because looking in the sky is like viewing a canvas. Nonetheless, the theoretical astrophysicist has to implement observational restrictions artificially to guarantee a valid comparison. This is the reason I look at optical richness in simulated galaxy clusters.

Optical richness plays a big role in the study of galaxy clusters, since the first 'photographs' of them (Wolf 1901). Max Wolf made a grid with every box representing the number of galaxies of the coma cluster in this area. Today Richness represents the number of luminous galaxies within a certain distance to the cluster center. Light in the visible wave lengths was the first accessible property for astronomers to observe. Naturally they began to categorize clusters depending on their morphology, richness being one possible way. Today, richness holds the opportunity to calculate masses for large samples of galaxy clusters, whereas the one present method through gravitational lensing is time consuming and not possible for arbitrary clusters. My task was to see if the mass richness relations found by observers fit my relations generated with the Magneticum simulations, showing that the concept of richness exists in the simulation self consistently and matches the observations. This would lead to a better comparison of cluster masses, which constrains the used cosmological parameters, enabling us to learn more about the early universe and its development in space and time.

Chapter 2

Theoretical Foundations

In this chapter I want to outline the knowledge needed to understand my work. It is divided into four parts, beginning with the basics of cosmology. Several of physical values will be derived that we will need in later chapters. The development of the universe, dependent on the cosmological constants is very fascinating. However it would lead too far from the actual subject of this thesis, namely galaxy clusters. Therefore I will leave that out.

The basic physics of galaxy clusters will be discussed in the second part of this chapter. I will present the four main matter components of galaxy clusters, being dark matter, intra cluster gas, stellar mass and black holes, and explain the physical effects they cause.

In the third and last section of this chapter I want to give a brief overview of the used numerical simulation, the Magneticum simulation.

2.1 Cosmology

Cosmology lays the foundations of the physics of large scale structures in the universe, galaxy cluster being one of them. Therefore we first have to understand how the space, which contains these large structures (our universe) can be described and what impact it has on the measurement of these objects, before we start discussing galaxy clusters in particular. Most of the formulae derived in this chapter are based on chapter 4 of 'Einführung in die extragalaktische Astronomie und Kosmologie' (Schneider 2015).

2.1.1 Redshift

We can measure the radial velocity of galaxies through the doppler shift of spectral lines. Doing so, we see that the radial velocities are positive for almost all galaxies. This leads to the impression, that they move cohesively away from us. Edwin Hubble determined a linear relation between the radial velocity v and the distance of the galaxies D:

$$v = H_0 D \tag{2.1}$$

The value of the constant is approx. $70 \frac{\text{km}}{\text{s Mpc}}$ and is the least known constant in astronomy. The confusion and problems this brings with it will be discussed in section 2.1.5. The redshift due to shift of spectral lines is defined as

$$z \equiv \frac{\lambda_{\text{obs}} - \lambda_0}{\lambda_0}, \ \lambda_{\text{obs}} = (1+z)\lambda_0, \tag{2.2}$$

where λ_0 is the wavelength of the spectral transition within the system of rest and λ_{obs} the observed wavelength. Today we know that this motion is due to the expansion of the universe. In section 2.1.4, this will be explained in detail. There we will see that the expansion can be described with a dimensionless factor a, the scale factor. Here it is important to note that the measured redshift is a combined redshift of this expansion and the actual radial velocity, due to gravitational interaction.

2.1.2 The Cosmological Principle

Cosmology describes our universe as a whole. Instead of the objects within our universe, time and space itself are the subject. Emphasis is placed on our, because other universes or 'our' universe before the big bang are not being discussed in cosmology. Having only one universe to make statements about is why cosmology differs from other disciplines. Our universe cannot be compared to other universes, because there is no way to measure it. Not even every point in our own universe can be observed. First of all the sensitivity of telescopes is limited, secondly the finiteness of light speed presents a limit. A look far away is a look into the past. It is thought, that the universe formed approx. $t_0 = 13,8$ Gyr ago. Therefore only points that are $r = ct_0$ away can be observed. Which defines our visible universe. Before the universe can be described in a quantitative manner, a few assumptions have to be made. The redshift measured for galaxies suggests that our universe is dynamic. Further assumptions are isotropy and homogeneity of the universe. Isotropy is based on the fact that on large scales the distribution of galaxies is nearly the same, independent of the direction looked from and the isotropy of the cosmic microwave background radiation explained in chapter 2.2.2. Homogeneity follows easily if considered that no point can be distinguished from others in our universe. Thus, it is isotropic around every point, which is the definition of homogeneous. Yet our universe looks anything like homogeneous to us. By

comparing the length of the largest measured structures in the universe of $\sim 100h^{-1}$ MPc to the Hubble - Length $R_H = \frac{c}{H_0} = 2997h^{-1}$Mpc it can be seen that substructures can be neglected in a cosmological context. The Hubble - Length represents the characteristic radius of the visible universe. The combination of homogeneity and isotropy is called the cosmological principle.

2.1.3 Critical Density

Gravitation is the dominant force in our universe and Newtonian gravitation describes our universe surprisingly well. Generally, it has to be assumed that space can be curved, therefore one would need general relativity. Nevertheless, a model universe can be created that is small enough to remain flat and deduce from the time development of this model universe, due to the assumed homogeneity, to the time development of our whole universe. Of course this is just an approximation, because substructure cannot be neglected at the same time as curvature, being the effects on the small respectively the large end of the scale, but it will help to understand it more easily.
Let us start by imagining a homogeneous sphere and allow it to expand in a manner, that the density $\rho(t)$ varies over time, but not in space. Now we pick a point in time $t = t_0$ and introduce a spatial coordinate system with origin in the center of the sphere. Due to expansion, the particle position $\mathbf{r}(t)$ is time dependent. Since the expansion is radial, the direction of $\mathbf{r}(t)$ is constant and the position can be written as

$$\mathbf{r}(t) = a(t)\mathbf{x}, \tag{2.3}$$

where $a(t)$ is called scale factor and meets $a(t_0) = 1$ by definition. It describes the dynamics of our universe. t_0 is arbitrary, therefore it is chosen to represent the present time. Observers, who move according to equation equation 2.3 are called comoving observers. The velocity of an observer due to the expansion is given by derivative in time of equation 2.3

$$\mathbf{v}(\boldsymbol{r}, t) = \frac{d}{dt}\boldsymbol{r}(t) = \frac{da}{dt}\boldsymbol{x} = \frac{\dot{a}}{a}\boldsymbol{r} \equiv H(t)\mathbf{r} \tag{2.4}$$

with $H(t_0) \equiv H_0$. To derive the time development of our universe we have to treat it dynamically by taking forces into account. Therefore we look again at a sphere with radius x at the time t_0 and a radius $r(t) = a(t)x$ for an arbitrary t. The included mass is independent of time and measures

$$M(x) = \tfrac{4\pi}{3}\rho(t)r^3(t) = \tfrac{4\pi}{3}\rho_0 x^3. \tag{2.5}$$

One can see that $\rho_0 = \rho(t)a^3(t)$. We can now formulate the equation of motion, knowing that the acceleration is mainly due to gravitational force and pointing inwards:

$$\ddot{r}(t) = -\frac{GM(x)}{r^2} = -\frac{4\pi G}{3}\frac{\rho_0 x^3}{r^2}. \tag{2.6}$$

This can be rewritten as

$$\ddot{a}(t) = -\frac{4\pi G}{3}\frac{\rho_0}{a(t)}. \tag{2.7}$$

Equation 2.7 is independent of x and thus only dependent on matter density. We can get another representation, by multiplying equation 2.7 with $2\dot{a}$:

$$\ddot{a}(t) \cdot 2\dot{a} = -\frac{4\pi G}{3}\frac{\rho_0}{a(t)^2} \cdot 2\dot{a} \Leftrightarrow \dot{a}^2 = \frac{8\pi G}{3}\frac{\rho_0}{a(t)} - Kc^2 \tag{2.8}$$

The left side is equivalent to the right side by integrating, where $-Kc^2$ is the integration constant. If we now multiply both sides with $\frac{x^2}{2}$ we get

$$\frac{v^2(t)}{2} - \frac{GM}{r(t)} = -Kc^2\frac{x^2}{2} \tag{2.9}$$

Equation 2.9 represents energy conservation, which allows to interpret the integration constant. Since K is proportional to the total energy, the evolution of the universe is dependent on K. Three cases can be distinguished:

- $K < 0$: The kinetic energy has to be always larger than the potential energy, thus our universe is endlessly expanding
- $K = 0$: The kinetic energy has to always be of the same norm as the potential energy. In this case our universe is endlessly expanding as well.
- $K > 0$: Now the kinetic energy can be zero for $a = a_{\max} = \frac{8\pi G\rho_0}{3Kc^2}$. In this case the universe stops expanding and collapses.

The special case of $K = 0$ separates the models of endless expansion from collapsing ones. From the right hand side of equation 2.8 it can easily be seen that $H_0^2 = \frac{8\pi G}{3}\rho_0$ for $K = 0$. Our universe has therefore a critical density of

$$\rho_{\text{crit}} = \frac{3H_0^2}{8\pi G} = 1.88 \cdot 10^{-29}\ \text{h}^2\text{g/cm}^3. \tag{2.10}$$

This physical quantity will be very important for characterizing galaxy clusters later on.

2.1.4 Cosmic Parameters

The Newtonian approach generates almost all important aspects of the homogeneous and isotropic world models. Nevertheless it is modified by general relativity in several ways: From special relativity we know that mass is equivalent to energy in terms of $E = mc^2$. This means that we do not only have to account for the density of matter in our equations of motion. Radiation generates energy densities, that correspond to matter densities according to this principle. Moreover these densities correspond to a pressure, if we put our universe into the first law of thermodynamics $dU = -PdV$:

$$\frac{d}{dt}(c^2\rho a^3) = -P\frac{da^3}{dt}. \tag{2.11}$$

Another change can be seen if we look at the equation of motion obtained by solving the relativistic field equations:

$$(\frac{\dot{a}}{a})^2 = \frac{8\pi G}{3}\rho - \frac{Kc^2}{a^2} + \frac{\Lambda}{3} \tag{2.12}$$

Λ is called the cosmological constant. The cosmological constants interpretation changed over time. Today it is thought to account for vacuum fluctuations of the universe. For example spontaneous pair production of electrons and positrons, within short time spans. For all forces those fluctuations cancel out, because of positive and negative charge. Gravitational force on the other hand is always attractive and thus creates a density field.

We now want to derive the equations of motion, including other forms of matter as well. Pressure of a gas is generally determined by the speed of its constituents and can be identified with an energy density. Summarized:

- dust - this is the matter described until now. Constituents have approx. the speed of sound and temperatures are quite low. For this gas holds $P \ll \rho c^2 \sim 0$
- radiation - not only including classic radiation like the cosmic background radiation, but also high speed particles, that meet $k_B T \gg mc^2$. This case results in the equation of state $P_r = \rho_v c^2$
- vacuum energy - we already discussed how vacuum fluctuations create an energy density. Note, that it has negative pressure. We get the equation of state $P_v = -\rho_v c^2$.

Let us derive the equations of motion again, first deriving both sides of equation 2.12 and then executing the derivatives in equation 2.11 to get an expression for $\dot{\rho}$. By coupling

$$2\dot{a}\ddot{a} = \frac{8\pi G}{3}(\dot{\rho}a^2 + 2a\dot{a}\rho) \tag{2.13}$$

and

$$\dot{\rho}a^3 + 3\rho a^2\dot{a} = -3Pa^2\dot{a}/c^2, \tag{2.14}$$

a pressure term appears in the equations of motion

$$\frac{\ddot{a}}{a} = -\frac{4\pi G}{3}(\rho + \frac{3P}{c^2}), \tag{2.15}$$

with

$$\rho = \rho_m + \rho_r + \rho_v, \;\; P = P_r + P_v \tag{2.16}$$

The same results can be obtained by identifying ρ with $\rho_m + \rho_r$ and ρ_v with

$$\rho_v = \frac{\Lambda}{8\pi G} \tag{2.17}$$

in the equations of motion firstly derived. Equations 2.12 and 2.15 are called the first and second Friedmann equation, respectively. In this formulation ρ_v is represented by Λ and not included in ρ. Time development of the densities is the next important step. It can be derived by taking the listed equations of state and putting them in the first law of thermodynamics (equation 2.11). For ρ_m this results in $\rho_m(t) = \rho_{m,0}a^{-3}(t)$, because the approximation for the pressure of dust with zero. Regarding the radiation this results in the equation

$$\frac{d(\rho_r a^3)}{dt} + \frac{\rho_r}{3}\frac{da^3}{dt} = 0. \tag{2.18}$$

This can be transformed to

$$d\rho_r a^3 = -\frac{4}{3}\rho_r da^3, \tag{2.19}$$

which can be integrated and results in $\rho_r(t) = \rho_{r,0}a^{-4}(t)$. From a physical point of view the interpretation is as follows: The number density of the photons changes equal to ρ_m with a^{-3}, whereas the energy of a photon changes with a^{-1}. This is because the energy of a photon is proportional to its wavelength, which will be redshifted. The energy density of vacuum is as mentioned a constant, which results in $\rho_v(t) = \rho_v$. This allows to formulate dimensionless constants, that represent the amount of total density distributed across the different types of "matter":

$$\Omega_m = \frac{\rho_{r,0}}{\rho_{\text{crit}}}, \;\; \Omega_r = \frac{\rho_{r,0}}{\rho_{\text{crit}}}, \;\; \Omega_\Lambda = \frac{\rho_v}{\rho_{\text{crit}}}, \tag{2.20}$$

with $\Omega_0 = \Omega_m + \Omega_r + \Omega_\Lambda$. With these cosmic parameters and the definition of the critical density 2.10 the expansion equation 2.12 reads

$$H^2(t) = H_0^2[a^{-4}(t)\Omega_r + a^{-3}(t)\Omega_m + a^{-2}(t)\Omega_K + \Omega_\Lambda], \tag{2.21}$$

where $\Omega_K = -\frac{Kc^2}{H_0^2}$. The scale factor $a(t)$ depends on the cosmological epoch. Let us derive an easy description of a, assuming a light beam that reaches earth today. This light beam is redshifted due to expansion of the universe on its way to earth. The infinitesimal redshift $dz = \frac{d\lambda}{\lambda}$ can be rewritten as $\frac{dv}{c}$. The difference in velocity is according to equation 2.4, so one obtains $\frac{dv}{c} = \frac{H}{c}dr = Hdt = \frac{da}{a}$. In the last two steps it is used that the light travels through space with light speed $\frac{dr}{dt} = c$ and the definition of the Hubble parameter in equation 2.4. This relation can be easily integrated resulting in $\lambda(a) = a\lambda_{\text{obs}}$, where λ_{obs} is the integration constant. At the time of emission applies $\lambda_e = a(t_e)\lambda_{obs}$ and with equation 2.2 the relation

$$a = \frac{1}{1+z} \tag{2.22}$$

is obtained. A lot of interpretations can now be made. But for this thesis, it is enough to describe the model universe and understand the equations for galaxy clusters. In my calculations, I used a flat universe ($\Omega_0 = 1, K = 0$) with the parameters

$$H_0 = 70,\ \Omega_m = 0.3,\ \Omega_\Lambda = 0.7 \text{ ,and } \Omega_r \text{ is negligible.} \tag{2.23}$$

2.1.5 Hubble Parameter

We learned that depending on how far an object is away from us (may it be in space or in time), its length varies due to the expansion of the universe, see equation 2.4. The Hubble parameter itself is dependent on redshift according to $H(z) = H_0E(z)$ with

$$E(z) = \sqrt{\Omega_R(1+z)^4 + \Omega_M(1+z)^3 + \Omega_K(1+z)^2 + \Omega_\Lambda}$$

Hence the dependence on redshift is known, provided the cosmic parameters were specified. Unfortunately, the Hubble constant is one of the least known values in astronomy and there have been furious debates about which value to use. Values ranged from 50 km s^{-1} Mpc^{-1} to 100 km s^{-1} Mpc^{-1}. This can lead to a lot of mistakes and misunderstandings. Furthermore, the dimensionless hubble constant h is defined as

$$H_0 = 100 \text{ h km s}^{-1} \text{ Mpc}^{-1}.$$

Debates resulted in the compromise to factor out the H_0 dependence is factored out and put in later on with the desired h value. It is important to note, that h is just a constant, not a unit, nor redshift dependent, although it often seems to appear as a unit. It itself solely depends on which measurement the authors views as most trustworthy. However it represents an uncertainty about a physical value, depending on how it is obtained. If we take the stellar mass of a galaxy cluster for example, we find either

$$M = 4.224 \cdot 10^{14}\text{h}^{-1}\text{M}_\odot \textit{ or } M = 2.973 \cdot 10^{14}\text{h}^{-2}\text{M}_\odot$$

Both represent the same value. However the left one is mostly seen as result of simulations. In simulations the mass can be calculated from the virial theorem and velocity dispersion according to $M_{tot} = \frac{R_{vir}\langle v^2\rangle}{G}$ (2.20). The radius scales with a and since h is factored out we have to divide by h to obtain the absolute value. The right one, on the other hand,

is seen in observations. They calculate mass from luminosity, which scales with the area, resulting in a dependence of h^2. For more examples see and a more detailed explanation see (Croton 2013). Knowing the different dependencies is very important to be able to compare simulated with observed data, like I do in chapter 3.

2.2 Physics of Galaxy Clusters

Galaxies are not evenly distributed in space - on the contrary: they show the tendency to gather in so called galaxy clusters (Schneider 2015). Despite what this name implies, galaxy cluster do not primarily consist of galaxies. Typical galaxy clusters have masses of about $\sim 10^{14} to 10^{15} \mathrm{M}_{\odot}$. Only about 5 % of their mass is due to galaxies. The bulk of mass is given by dark matter ($\sim 65 to 85\%$) and most of the remaining mass comes from intracluster gas ($\sim 10 to 30\%$)[1]. In the following sections I want to present the cluster components in detail. We will see that galaxy cluster's size is of order of a few Mpc and that they are assumed to sit at the nodes of filaments in the cosmic web. Most of my information for this chapter can be found in Sarazin 1988 [2], otherwise I will state the source separately.

2.2.1 Dark Matter (DM)

Cluster masses were first derived by Zwicky (1933) and Smith (1936). They found that the masses greatly exceed those which would be expected by summing the masses of all the cluster galaxies. The masses of galaxy clusters can be determined if it is assumed that they are bound, self-gravitating systems. If they were not, they would disperse rather quickly ($\sim 10^9$ yrs). Therefore the limit on the mass of clusters comes from the binding condition,

$$E = T + V < 0 \tag{2.24}$$

where E represents the total energy, T the kinetic energy and V the gravitational potential energy. If this condition holds true, the system can be considered as virialized. Furthermore, a radius can always be found within the cluster for equation 2.24 being met. This radius is called the virial radius. Given the Newtonian gravitational potential, the virial theorem provides the relations

$$V = -2T, \; E = -T$$

With these relations, the aforementioned potential and the classical kinetic energy the relation

$$M_{\mathrm{tot}} = \frac{R_{\mathrm{vir}} \langle v^2 \rangle}{G} \tag{2.25}$$

is obtained. Assuming that the velocities of the galaxies are uncorrelated one can write $\langle v^2 \rangle = 3\sigma_r^2$, where σ_r is the radial velocity dispersion. σ_r can be measured due to the redshift of galaxies within a cluster and R_{vir} can be measured in several ways (projected separation, fit to galaxy distribution). This results indeed in $M_{\mathrm{tot}} \sim 7 \cdot 10^{14}$ solar masses. It appears to be quite a challenge to indicate a cluster's size, since the gravitational force is proportional to $\frac{1}{r^2}$ and is for this reason always larger than zero. R_{vir} is one of the values that represent a cluster's size, which is about a few Mpc. If a system is expected to completely consist of stars, a mass to light ratio like the sun's should be expected. However, mass to light ratios are found, that are of about two orders of magnitude higher than expected (Rood 1981). This "missing mass", that only interacts gravitationally and does not emit radiation, is what is called dark matter (everything else is called baryonic matter). Therefore it can only be measured indirectly. The nature of dark matter is still an unsolved question in current research and there are various elementary particles, that are discussed (Garrett and Duda 2010). Because dark matter only interacts gravitationally, it had the possibility to form potential wells in the early universe.

[1] http://www2.astro.psu.edu/~caryl/a480/lecture12_10.pdf
[2] https://ned.ipac.caltech.edu/level5/March02/Sarazin/frames.html

2.2.2 Intra Cluster Medium (ICM)

Galaxy clusters are among the brightest sources of X-ray radiation (Schneider 2015). The area that emits this radiation is extended over the whole cluster and does not come from single galaxies. Characteristic luminosities are about $L_X \sim 10^{43-45} erg/s$. Fig. 2.1 shows typical spectra at different temperatures with solar element abundances. The lower two graphs fit the observed spectrum of galaxy clusters the best. We can therefore conclude that the temperature of the intra cluster gas is about $10^{7-8} K$. Three emission processes involving electronic interaction contribute to the radiation: bremsstrahlung radiation caused by the acceleration of an electron in the coulomb field of an ion, recombination radiation caused by the capture of an electron by an ion following ionization, and deexcitation radiation of an electron lowering the quantum state in an atom. The first two processes generate continuum radiation and the latter line radiation. As can be see, the dominant radiation process in galaxy clusters is bremsstrahlung. This is because of the fact that at these temperatures hydrogen and helium are fully ionized and only interact with electrons in a way of deflection. Nevertheless elements like iron are not fully ionized. The deexcitation of 25 times ionized iron (an iron nucleus with one electron) produces enough energy (about $7keV$) to be seen in the spectrum. Due to the very low densities in the ICM of about 10^{-3} particles per cubic centimeters, there are even radiative transitions of electrons that would be forbidden otherwise. The low densities are also the reason why so much X-ray radiation can escape the ICM without being absorbed.

Another interesting effect that is caused by the ICM is the inverse compton scattering of the cosmic background radiation (CMB), first described by Sunyaev and Zel'dovic (1980).

Right after the big bang the density was so high that the mean free path length was too short for the photons to escape. The universe began to cool down and recombination processes caused the medium to become transparent for photons. This is the oldest radiation of the universe we can measure and it is called cosmic microwave background radiation. Given the cosmological principle, one would also expect it to be isotropic. This is not exactly the case. The main anisotropy originates in quantum fluctuations of the early universe. Another minor anisotropy is caused, because on its way to us the CMB photons traverse the intra cluster gas of several galaxy clusters. The photons are scattered to higher energies by the hot electrons in the gas.

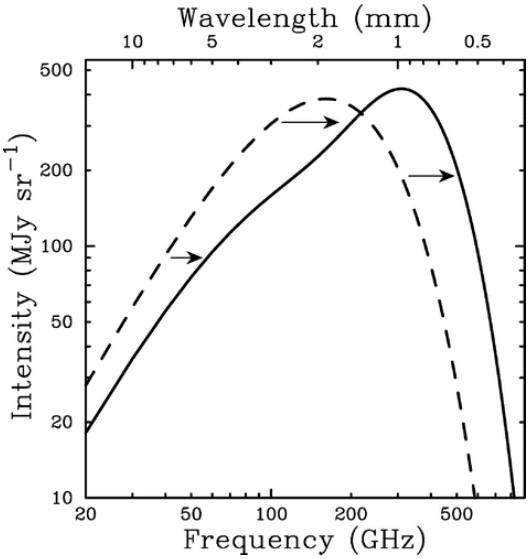

Figure 2.2: Graphic, that shows how SZE influences the CMB [3]

Non - thermal radiation of clusters is mainly due to merging effects. At high redshifts, where we can see elongated, asymmetric structures of galaxy clusters effects like turbulence, shocks, streaming motions and cold fronts can be measured.

[3] source: `https://ned.ipac.caltech.edu/level5/Sept05/Carlstrom/Carlstrom2.html19.07.2017`

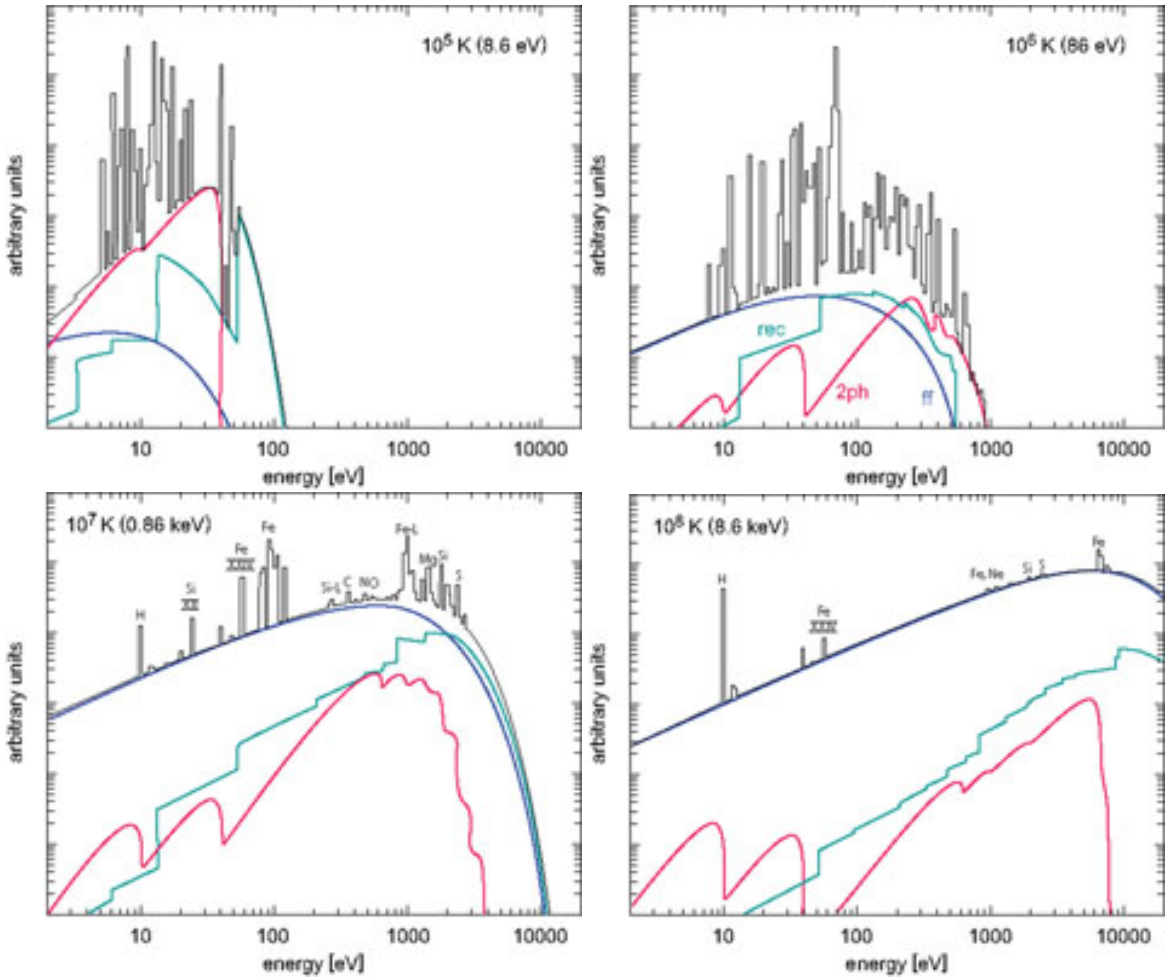

Figure 2.1: X-ray spectra for solar abundance at different plasma temperatures. The continuum contributions from bremsstrahlung (blue), recombination radiation, characterized by the sharp ionization edges (green), and 2-photon radiation (red) are indicated. Source: `https://ned.ipac.caltech.edu/level5/Sept09/Bohringer/Bohringer2.html19.07.2017`

Figure 2.3: *left panel:* The galaxy cluster Abell1689 in the visible spectrum. Source: `https://www.jpl.nasa.gov/spaceimages/details.php?id=PIA10237` *right panel:* Our neighbor galaxy, the Andromeda galaxy (M31) in the visible spectrum. Source: `https://apod.nasa.gov/apod/ap130626.html`

2.2.3 Stellar Component

Even though the stellar component makes up for only $\sim 1\%$ of a cluster's mass it plays a big role in observations, especially in earlier studies of galaxy cluster, because the stellar component emits the bulk of light in the visible spectrum. Observers began to classify cluster morphology according to their 'richness'. There are several ways to define richness. The one I used for my research reads as follows

Richness is the absolute number of galaxies within the radius R_{200} of a cluster, that are at least as luminous as 40% of the luminosity of the Milky Way. (Rykoff et al. 2008)
There are a lot of other classification schemes for morphological types of clusters summa-

Table 2.1: Summary of various schemes to classify morphological types of galaxy clusters

Property	Regular	Intermediate	Irregular
Zwicky Type	Compact	Medium-Compact	Open
Richness	Rich ($\sim 10^2$)	Rich-Moderate ($\sim 10^1$)	Rich-Poor ($\sim 10^0$)
Symmetry	Spherical	Intermediate	Irregular
Central Concentration	High	Moderate	Low
Subclustering	Absent	Moderate	Significant

rized in table 2.1. These systems of classification are empirically found to be highly correlated, and can roughly be mapped into a one-dimensional sequence running from regular clusters to irregular clusters. These correlations indicate a connection between the dynamical state and galactic content of clusters. There is no one-to-one correlation between the morphology of a cluster and its richness. Regular clusters are always rich, while irregular clusters may be either rich or sparse. Nevertheless, observers classify their observed clusters in richness groups for a better comparison. Regarding the galaxies in galaxy clusters, they are mostly diffuse ellipticals, due to the high merger activity. Galaxies in clusters are often quenched and therefore form less stars, than field galaxies. This is why M31 seems more bluish than the galaxies in Abell1689. A comparison between a field galaxy and cluster galaxies can be seen in fig. 2.3.

2.2.4 Black Holes, Active Galactic Nuclei (AGN)

It is generally accepted that present-day spheroidal galaxies host supermassive black holes (BHs) at their centres (Magorrian et al. 1998). In addition, strong correlations are found between BH masses and properties of their host galaxies as the bulge mass, the stellar velocity dispersion and the X-ray luminosity. This can be interpreted as an evidence for a co-evolution between the spheroidal component of host galaxies and their BH's. During their lifetime, BHs are assumed to undergo several episodes of significant gas accretion, during which this accretion powers active galactic nuclei (AGN) (Salpeter 1964). In fig. 2.4 a sketch of the unified scheme of AGN structure is displayed. Because the lengths are not true to scale, real sizes are listed in table 2.2. Friction in the accretion disk of the AGN causes high temperatures and a lot of energy is radiated away. Magnetic fields are twisted and generate a pointed mass outflow called jet. These jets consist of high velocity particles, that can increase the temperature of the surrounding inter galactic medium. The jet is responsible for the bulk of measured radiation in the radio wavelength, but an AGN emits enormous radiation across the whole electromagnetic spectrum.

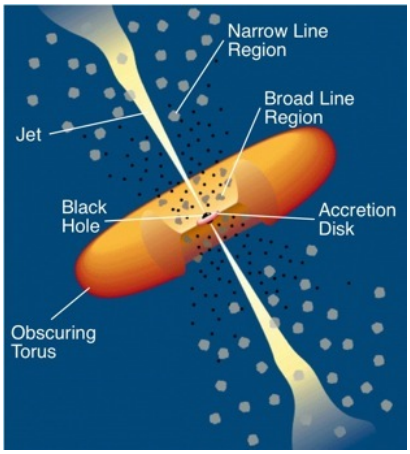

Figure 2.4: The unified scheme of AGN structure (Padovani 1997)

AGN component	Size
black hole	$10^{-7}pc$ to $10^{-4}pc$
accretion disk	$\sim 10^{-3}pc$
broad line region	$0.01pc$ to $0.1pc$
torus	$0.1pc$ to $10pc$
narrow line region	$100pc$ to $1000pc$
jets	$1kpc$ to $1Mpc$

Table 2.2: Length scales of AGN components.

The impact such AGN's have on the luminosity of clusters will become important for my analysis, so let us discuss them in detail. The following derivation is taken from a lecture at Oxford University [4]. Every luminous object in the universe has a maximum luminosity, beyond which radiative pressure will overcome gravitational pressure and material outside of the object will rather be pushed away than accreted. Let us consider an object of radius R and mass M. The gravitational force an object feels at R is given by Newton's law. The outwards pointing radiation force is given by

$$F_{\mathrm{rad}} = P_{\mathrm{rad}} \kappa m$$

where κ is the opacity, meaning the cross-sectional area per unit mass for radiation scattering and P_{rad} the radiative pressure given by

$$P_{\mathrm{rad}} = \frac{L}{c} \frac{1}{4\pi R^2}$$

[4]Source: `http://www-astro.physics.ox.ac.uk/~garret/teaching/lecture7-2012.pdf`

balancing the forces and solving for L results in the Eddington - Luminosity.

$$L_{\text{Edd}} = \frac{4\pi GMc}{\kappa}$$

Assuming to be in the regime of high energy accretion, the accreted particles can be approximated to be mostly ionized hydrogen. Therefore the opacity comes mostly from radiation pressure on electrons, whereas the mass comes from the protons. Although the radiation is mostly felt by electrons, they will drag the protons with them, because of electro static forces. Hence we approximate $\kappa = \frac{\sigma_T}{m_p}$, where σ_T is the Thomson cross - section and obtain

$$L_{Edd} = \frac{4\pi GMcm_p}{\sigma_T}.$$

This luminosity is the result of accreted mass, whose gravitational potential energy is transformed to some degree into radiation energy. Suppose an accretion rate of $\dot{M}$ and a fraction ϵ that expresses how much energy is radiated away, we get

$$L = \epsilon \dot{M} c^2.$$

Since there is a maximum luminosity given by L_{Edd}, $\dot{M}$ is limited from above as well. Setting both equations for the luminosity equal and solving for $\dot{M}$ results in

$$\dot{M}_{Edd} = \frac{4\pi M m_p}{\epsilon c \sigma_T}$$

This is the Eddington - accretion rate. If $\dot{L}/\dot{L}_{\text{Edd}} \sim 1$ the object is called radiatively efficient. If it is < 0.1, it is called radiatively inefficient. Even if the black hole emits a lot of radiation, it is not guaranteed to contribute to the cluster's luminosity. The black hole can be obscured because of gas clouds that absorb most of the radiation.

2.3 Numerical Simulations

Modern cosmological observations allow astrophysicists to study the evolution and history of large scale structure hierarchy in great detail. Accurate constraints on the cosmological parameters within a given cosmological model is a fundamental problem which requires precise modeling of the observed structure. Large-scale cosmological simulations utilizing modern supercomputers are essential tools for accurately calculating theoretical predictions of the distribution and state of the baryonic and dark matter in the Universe. Especially in the non-linear regime of gravitational dynamics and hydrodynamics, where galaxies and clusters of galaxies form out of the large scale structure, they are of greatest importance.

Throughout all of my thesis I used the Magneticum pathfinder simulations (Dolag et al in prep). The Magneticum pathfinder simulations are hydrodynamical simulations based on the extended version of the parallel TreePM SPH-code GADGET-2 (Springel 2005) called P-GADGET-3. For dark - matter - only simulations an N-body code would suffice, however particle-particle interaction plays a tremendous role in the interaction of baryonic matter, which needs a hydrodynamical treatment. Many physical effects are included in the Magneticum pathfinder simulations[5]:

- cooling, star formation, winds
- Metals, stellar population and chemical enrichment SN-Ia, SN-II, AGB new cooling tables
- Black holes and AGN feedback
- Thermal Conduction
- Low viscosity scheme to track turbulence
- Magnetic Fields (passive)

The Magneticum Pathfinder simulations are hydrodynamical cosmological simulations that cover box sizes up to Gpc^3 in yet unaccomplished detail. Six different boxes of varying sizes and resolution allow the multiple wavelength comparison to observed data. I restrict myself to Box 2b. With a size of $(640Mpc)^2$ it allows to study galaxy clusters in a cosmological context and a high resolution of $2 \cdot 2880^3$ particles allows to take astrophysical processes reliably into account. Dark matter particles have masses of $6.9 \cdot 10^8 M_\odot/h$ and gas particles have masses of $1.4 \cdot 10^8 M_\odot/h$ with softenings of $10kpc/h$ to avoid diverging of forces if the simulated particles get too close. The simulation started at redshift $z = 60$ and evolved to $z = 0.25$. I mostly used the snapshot with lowest redshift because I compared my results to observations of nearby clusters. The Magneticum pathfinder simulations use a ΛCDM cosmology taken from Komatsu et al. 2010, with the cosmological parameters $\Omega_0 = 0.272,\ \Omega_\Lambda = 0.728,$ and $H_0 = 70.4$.

[5] `http://www.magneticum.org/simulations.html`

Chapter 3

Creating Scaling Relations

Scaling Relations put two different physical quantities into context. Depending whether a correlation from one to the other can be found, the resulting curve can be used to associate one property with the other. In theoretical astrophysics scaling relations are crucial to test the numerical simulation. The simulation is a good representation of reality if the numerical relations fit the observed. Furthermore, it is important to see how observed scaling relations differ from theoretical, gravitational scaling relations to learn to what extend these are affected by hydrodynamical processes.

I want to begin this chapter by outlining how galaxy clusters in the simulation are found. This leads to a discussion of the Friend-of-Friend algorithm and the overdensity parameter. Results of scaling relations for the most important mass proxies, being temperature, X-ray luminosity, SZE, velocity dispersion and richness, will be discussed in the second section. These are calculated using the on-the-fly postprocessing of the simulation. In the third section I will examine how the results change by taking more physical processes into account, though I will restrict myself to the mass - luminosity relation. Luminosities will now be calculated with the program SMAC and the effect of AGN will be taken into account.

3.1 Galaxy Clusters in Magneticum

As the simulation ran, snapshots were created that represent the universe at a specific time. All physical properties can be calculated from these snapshot files, while many of them are directly obtainable through a postprocessing routine. The postprocessing routine generates huge arrays that store data like velocities, positions, but also indices e.g. to see what subhalo belongs to which halo.

Further I will refer to galaxies and galaxy clusters represented in the simulation as subhalos and halos, respectively. The reason is following: Galaxies and galaxy clusters in numerical simulations are represented by accumulations of particles. First of all the so-called friends-of-friends (FoF) algorithm is used to find all particles in a certain overdensity that are within a specific distance, the linking length, to another particle. Friends of friends are friends again, thus a halo is formed. Then, the SUBFIND algorithm searches for local minima in the halo potential. The local minima represent subhalos of the halo. It is hard to distinguish between halos that are close to each other or even merging. Because of numerical errors of this kind it is important to differentiate between clusters and halos. Furthermore halos and subhalos are general concepts. Depending on the mass threshold, a halo can represent something between groups of galaxies and galaxy superclusters.

It is important to note, that all physical quantities depend on the used radius for the cluster. Since there is no end to a cluster in a sense like an edge, their size is defined with the overdensity parameter Δ:

$$r_{\Delta}^{3} = \frac{3}{4\pi\rho_{crit}\Delta} M_{\text{cluster}}(r \leqslant r_{\Delta}). \tag{3.1}$$

This equation holds for different redshifts and even cosmologies, because in a self similar model the ratio of mean protocluster density to the background density at turnaround is the same for different redshifts.Which means that the cluster collapse is just scaled to higher densities for higher redshifts (Böhringer, Dolag, and Chon 2012). Furthermore a local region of the universe evolves like a universe with these local density and expansion parameters irrespective of the embedding cosmology according to the Birkhoff theorem.

Physical properties are calculated by the postprocessing within six radii r_{Δ}. These are the virial radius, the radius where the density is: 200/500 times the mean density of the universe and 200/500/2500 times the critical density of the universe ($\Delta = 200/500/2500$). Therefore it is very important to pay attention to the used properties in observations for a valid comparison. Furthermore one has to pay attention to the underlying cosmological parameters, since the physical properties behave differently at larger redshifts for different universes.

3.2 Mass Scaling Relations

The theoretical scaling relations I will present for each physical property are based on dark matter structure evolution with the assumption, that the baryonic matter follows the dark matter. Because hydrodynamical effects are neglected, they may differ from the scaling from observations and the simulation, but visualize quite well why there should be a scaling in the first place. Generally the radius of clusters scales with mass in a simple geometric way. Concerning the time development we have to look at the time dependence of the mean density (Böhringer, Dolag, and Chon 2012):

$$\frac{\rho_{crit}(z)}{\rho_{\rm crit}(z=0)} = \frac{H(z)^2}{H_0^2} = E(z)^2. \tag{3.2}$$

The evolution of the radius at fixed overdensity (eg. $\Delta = 500$) is therefore given by

$$r_{500} \sim (\frac{M_{500}}{\rho_0})^{1/3} \sim M_{500}^{1/3} E(z)^{-2/3}. \tag{3.3}$$

In this approach it is assumed that clusters have just collapsed and baryonic matter follows dark matter, which is only true in a very broad sense.

Table 3.1: Cluster properties. Taken from Pratt, Croston, et al. 2009. Mass calculated from SZE taken from Planck survey

name	T	L_X	Y_X	M_Y	z
RXC J0006.0-3443	5.03	4.13	22.74	3.77	0.11
RXC J0020.7-2542	5.69	6.52	22.41	4.56	0.14
RXC J0145.0-5300	5.53	5.00	26.62	3.49	0.11
RXC J0345.7-4112	2.19	0.77	1.91	1.78	0.06
RXC J0547.6-3152	6.02	8.97	35.54	5.30	0.15
RXC J0605.8-3518	4.56	9.54	22.39	5.40	0.14
RXC J0645.4-5413	6.95	18.88	71.61	7.87	0.16
RXC J0958.3-1103	5.18	11.56	28.04	5.18	0.17
RXC J1141.4-1216	3.31	3.75	8.60	3.27	0.12
RXC J1302.8-0230	2.97	1.38	6.07	2.83	0.08

Columns: (1) cluster name;(2) T: spectroscopic temperature of the $R < R_{500}$ region in keV;(3) Luminosity in the $R < R_{500}$ region in $10^{44} erg\ s^{-1}$;(4) Y_X in the $R < R_{500}$ region in units of $10^{13} M_\odot\ keV$;(5) M_Y in the $R < R_{500}$ region in $10^{14} M_\odot$;(6) cluster redshift.

3.2.1 Mass - Temperature

The first basic scaling is given by linking cluster mass to cluster temperature. The heat comes from the conversion of potential energy during the formation of the cluster (Böhringer, Dolag, and Chon 2012), resulting in

$$T \sim \Phi_0 \sim (\frac{M_\Delta}{r_\Delta}) \sim M_\Delta^{2/3} E(z)^{2/3} \Delta(z)^{1/3} \tag{3.4}$$

The comparison between observed and simulated mass - temperature scaling is shown in Fig. 3.1. The fitting function was taken from Ilić, Blanchard, and Douspis 2015

$$T = A_{TM} (hM_v)^{\beta_T M} (\frac{\Omega_m \Delta}{178})^(1/3)(1+z)^{1+\alpha_{TM}} \tag{3.5}$$

Figure 3.1: *Left panel:* Temperature - Mass scaling for galaxy clusters. Every black dot represents a halo from the MAGNETICUM simulation at redshift $z = 0.25$. The black curve is fitted to every single halo with the same error and the black diamonds represent the binned medians in constant steps of $1.5 \cdot 10^{13} M_{\odot}$. The green line displays the scaling relation from Ilić, Blanchard, and Douspis 2015, which is fitted to observed data. The green diamonds represent ten observed clusters listed in Table 3.1. *Right panel:* Residual plot displaying the weighted difference between the observed and the simulated scaling relation.

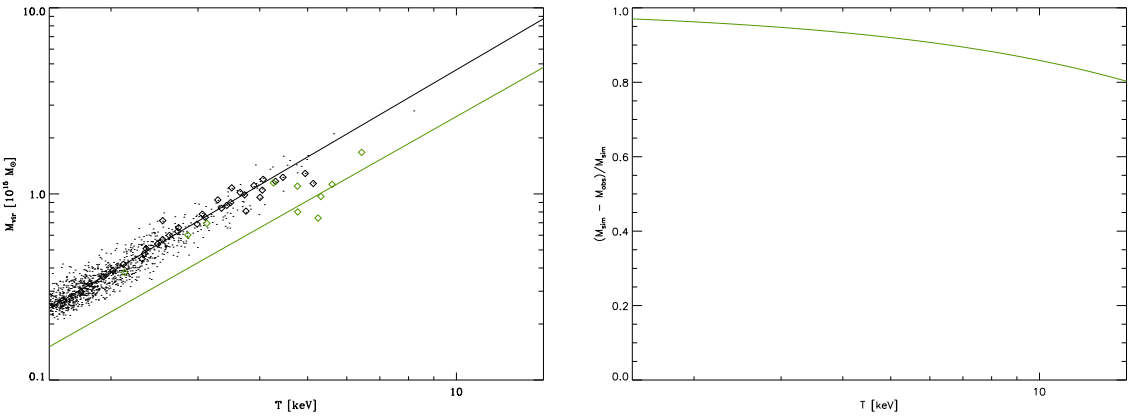

I created the simulation curve with this function using $\Omega_m = 0.3, h = 0.7$ and $\Delta = 200$ (concerning the cosmological parameters, this applies to the calculation of all physical properties). Ilié et al. calculated them more precisely to $\Omega_m = 0.316$ and $h = 0.67$. I set $z = 0.25$ for my curve and $z = 0.12$ for the observed curve, for a better comparison with the ten galaxy clusters (see table 3.1 for redshifts). The masses for these clusters are given in R_{500}, which is the reason why they must be multiplied by $\eta = 1/0.47054$. η is the mean residual between M_{200} and M_{500} in the simulation. The fitting resulted in $A_{TM} = 7.29$ ($\beta_{TM} = 0.67$ was put into the relation) for the observers and $A_{TM} = 8.08$, $\beta_{TM} = 0.606$ for the simulation. I fitted it directly without using logarithms resulting in a $\Delta\chi^2 = 185.8$ and $DOF = 1498$. Indeed, the observed clusters are more accurately fitted by the observer scaling relation. Nevertheless the residual is quite small and increasingly smaller for higher temperatures as can be seen in the right panel of fig. 3.4. Furthermore the slope of the scaling fits the theoretically assumed quite well.

3.2.2 Mass - Luminosity

According to (Henry and Tucker 1979) the temperature - potential relation can be expressed as $kT \propto Gm_H \rho_x(0) a_x^2$ with the central density (ions + electrons) $\rho_x(0)$ and the core radius a_x. Assuming galaxy clusters to be self gravitating isothermal spheres we obtain with the upper relation

$$L_x \propto n_x^2 V T^{1/2} \propto \rho_x(0)^2 a_x^3 T^{1/2} \propto T^{5/2} a^{-1} \tag{3.6}$$

This results in L_x being proportional to M, because the core radius a_x is proportional to the cluster radius and T is proportional to M according to Equ. 3.4. It is important to mention that clusters cannot be approximated by self gravitating isothermal spheres, because the cluster mass is dominated by dark matter, that does not emit radiation. However, an isothermal sphere confined by mass other than its own, describes a cluster quite well. Thus ρ_x has to be replaced by the fraction $\rho_x(0)/\rho_T(0)$ with the confining mass density $\rho_T(0)$. The distribution of dark matter and gas is approximately the same and $\rho_T(0) \sim 10\rho_x(0)$, thus

Figure 3.2: *Left panel:* Luminosity - Mass scaling for galaxy clusters. Every black dot represents a halo from the MAGNETICUM simulation at redshift $z = 0.25$. The black diamonds represent the binned medians in constant steps of $1.5 \cdot 10^{13} M_{\odot}$. The black curve is fitted to these medians. The red line displays the scaling relation from Pratt, Croston, et al. 2009, which is fitted to observed data. The red diamonds represent ten observed clusters listed in Table 3.1. *Right panel:* Residual plot displaying the weighted difference between the observed and the simulated scaling relation.

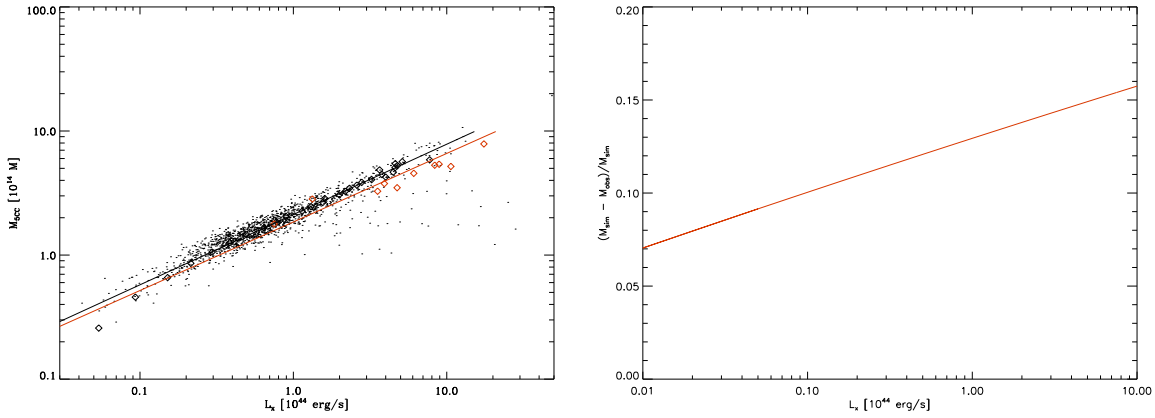

resulting in $L_x \propto M^{11/12}$. The comparison between observed and simulated luminosity - mass scaling can be seen in fig.3.2. The fitting function was taken from Pratt, Croston, et al. 2009:

$$h(z)^n L_X = C(A/A_0)^{\alpha}, \tag{3.7}$$

with $h(z) = hE(z)$, $A_0 = 2 \cdot 10^{14} M_{\odot}$, $n = -7/3$ and M_{ν} being the virial mass. This fitting method resulted in $\alpha = 1.81$, $C = 1.81$ for observed scaling and $\alpha = 2.00$, $C = 1.76$ for the simulated data. The values for $\Delta\chi^2 = 31.66$ and $DOF = 27$ changed drastically, because I now fitted the medians, due to the big scatter. The observational and simulation curve match each other surprisingly well, with residuals of 0.2 for small L_X and only 5% for high L_X. The slope is way higher than what one would expect seeing the theoretical relation. This means that hydrodynamical effects play a huge role in the emission of X-rays.

3.2.3 Mass - SZ

The SZ flux integrated within a certain radius, Y_{SZ}, is proportional to the total thermal energy of the ICM gas and thus to the overall cluster potential, which makes it relatively insensitive to the details of the ICM physics and merging (Kravtsov, Vikhlinin, and Nagai 2006):

$$Y_{SZ} = (\frac{k_B \sigma_T}{m_e c^2}) \int_V n_e T_e \, \mathrm{d}V \propto M_g T_m, \tag{3.8}$$

where k_B, σ_T, m_e and c have their usual meaning, n_e, T_e are the number density and temperature of the electrons respectively and T_m is the mass-weighted mean temperature of the ICM. With $M_{\Delta} \propto M_g$ and 3.4 one obtains

$$M_{\Delta} \propto Y_{SZ}^{3/5} E(z)^{3/2} \tag{3.9}$$

In fig.3.3 the comparison between observed and simulated SZ - Mass scaling is displayed.

Figure 3.3: *Left panel:* SZ - Mass scaling for galaxy clusters. Every black dot represents a halo from the MAGNETICUM simulation at redshift $z = 0.25$. The black curve is fitted to every single halo with the same error and the black diamonds represent the binned medians in constant steps of $1.5 \cdot 10^{13} M_{\odot}$. The teal line displays the scaling relation from Bocquet et al. 2014, which is fitted to observed data. The teal diamonds represent ten observed clusters listed in Table 3.1. *Right panel:* Residual plot displaying the weighted difference between the observed and the simulated scaling relation.

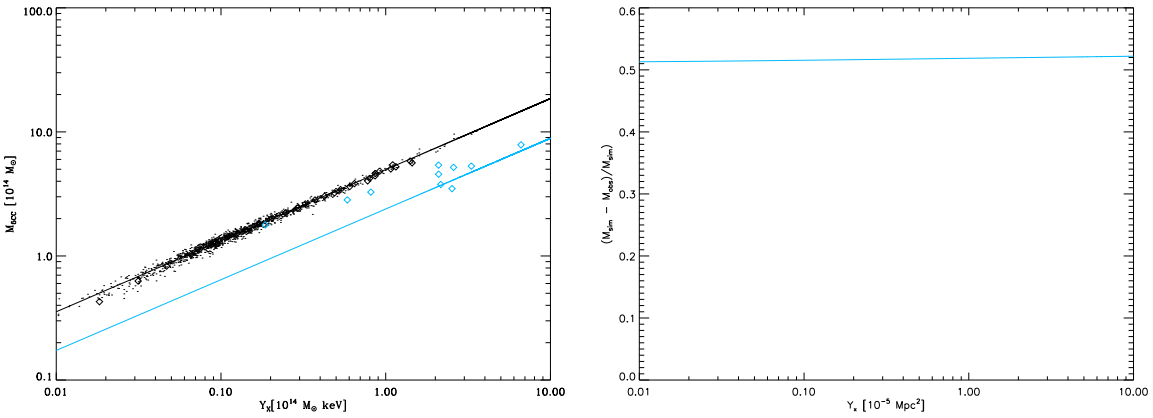

The fitting function was

$$\frac{M_{500,c}}{10^{14} M_{\odot}} = A_X h^{1/2} \left(\frac{Y_X}{3 \cdot 10^{14} M_{\odot}\ keV}\right)^{B_X} E(z)^{C_X}, \tag{3.10}$$

with the normalization A_X, slope B_X and redshift evolution parameter C_X. I used the observational $C_X = -0.4$ to guarantee a better comparison. This method resulted in $A_X = 5.77, B_X = 0.57$ for the observational curve and $A_X = 9.85, B_X = 0.57$ for the simulation curve. As we can see the scatter is phenomenally small, thus $\Delta\chi^2 = 0.96$ and $DOF = 1498$. It is remarkable that the residual is constant and represents a value close to $1/h$. Both fits reproduce almost exactly the slope that was to expect from the theory, making the relation indeed quite independent to hydrodynamics.

3.2.4 Mass - Velocity Dispersion

The relation between velocity dispersion and cluster mass was already derived in Chapter 2.2.1 being

$$\langle v_{1D} \rangle = \sqrt{\frac{2GM}{3R}}. \tag{3.11}$$

With Equ. 3.2 one obtains

$$\sigma \propto M_{500}^{1/3} E(z)^{1/3}. \tag{3.12}$$

I calculated the velocity dispersion in the following way

$$\sigma_{1D} = \frac{1}{\sqrt{3}} \sqrt{\langle (\mathbf{v_i} - \tilde{\mathbf{v}}_\mathbf{i})^2 \rangle}, \tag{3.13}$$

with $\tilde{\mathbf{v}}$ being the velocity of the central subhalo, and $\mathbf{v}$ being the velocities of the satellite galaxies. The comparison between observational and simulated scaling of velocity

Figure 3.4: *Left panel:* Velocity Dispersion - Mass scaling for galaxy clusters. Every black dot represents a halo from the MAGNETICUM simulation at redshift $z = 0.25$. The black curve is fitted to every single halo with the same error and the black diamonds represent the binned medians in constant steps of $1.5 \cdot 10^{13} M_\odot$. The purple line displays the scaling relation from Bocquet et al. 2014, which is fitted to observed data. The purple diamonds represent five observed clusters listed in Table 3.2, whose masses were multiplied by 1/0.4705 to get M_{200} approximately.*Right panel:* Residual plot displaying the weighted difference between the observed and the simulated scaling relation.

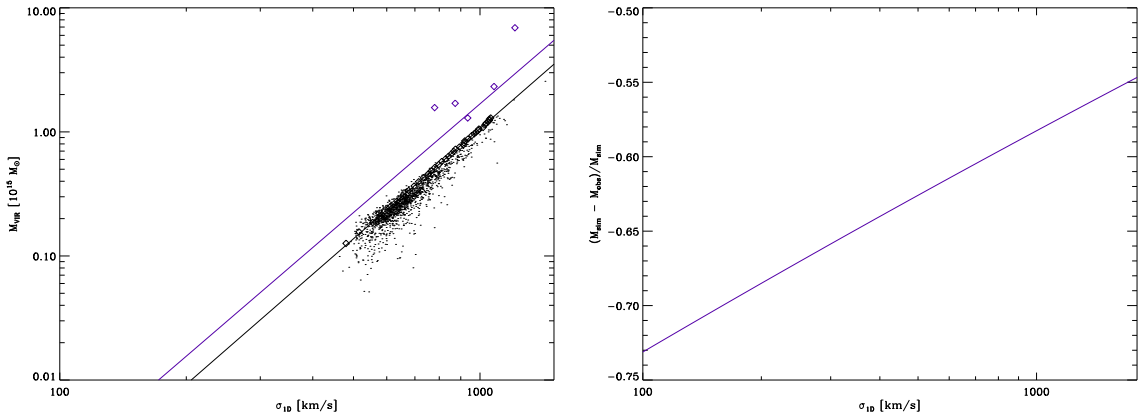

Table 3.2: Cluster properties. Taken from Ruel et al. 2014.

SPT-CL	J0000-5748	J0511-5154	J0438-5419	J0546-5345	J2058-5608
$M_{500,c}$	4.29	5.63	22.88	7.69	5.02
σ	935	873	1211	1080	780

rows: (1) cluster name; (2) $M_{500,c}$: Mass in the $R < R_{500}$ region in $h^{-1} M_\odot$; (3) σ: velocity dispersion in $km\ s^{-1}$.

dispersion and mass is depicted in fig. 3.4. The fitting function was

$$M_{200,c} = \left(\frac{\sigma}{A_\sigma h(z)^{C_\sigma}}\right)^{B_\sigma}\ 10^{15} M_\odot, \tag{3.14}$$

with the redshift evolution parameter $C_\sigma = 0.33$, which I used for my fitting as well, to get a better comparison. The fitting resulted in $A_\sigma = 939, B_\sigma = 2.91$ for the observational curve and $A_\sigma = 1100, B_\sigma = 2.95$ for the simulation curve. The scatter for this relation is comparatively big. Nevertheless $\Delta\chi^2 = 0.11$ and $DOF = 1498$. The masses of the observed clusters are quite big, but are indeed fitted better by the observational curve. The residual is big as well, but gets smaller for higher velocity dispersions. Both slopes are very close to the theoretical value of $B_\sigma = 3$. Both of them are just a little bit smaller, which may be due to friction effects.

3.2.5 Mass - Richness

Richness is a mere empirical property, that exists since the very first cluster catalog (Abell 1958). Therefore there is no way to analytically derive a scaling between mass and richness. However it is pretty clear that if a cluster has more and brighter galaxies in its center, it is also more massive. Yet, this makes it so interesting to look at in simulations, to see whether the implemented hydrodynamics suffice to generate a similar scaling.

Figure 3.5: *Left panel:* Richness - Mass scaling for galaxy clusters. Every black dot represents a halo from the MAGNETICUM simulation at redshift $z = 0.25$. The black curve is fitted to every single halo with the same error and the black diamonds represent the binned medians in constant steps of $1.5 \cdot 10^{13} M_{\odot}$. The blue line displays the scaling relation from Andreon and Hurn 2010, which is fitted to observed data. The blue diamonds represent the eight measured means listed in Table 3.2. *Right panel:* Residual plot displaying the weighted difference between the observed and the simulated scaling relation.

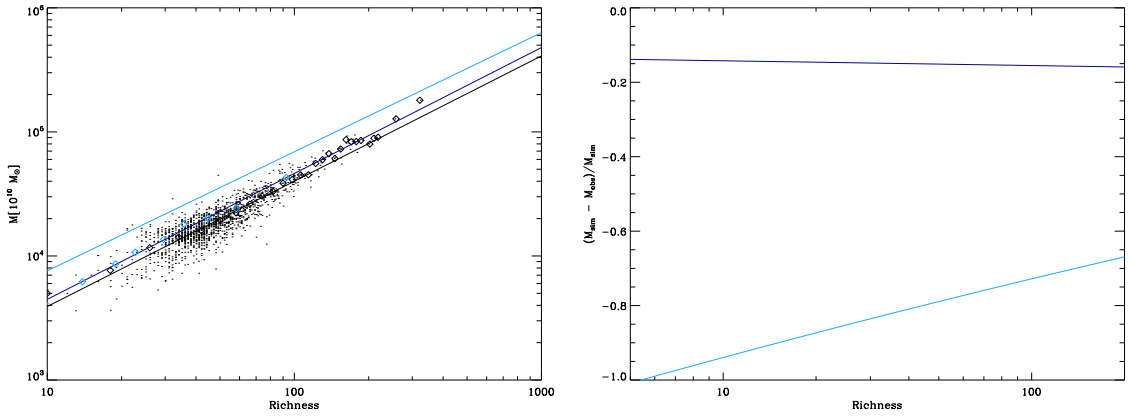

I calculated the richness for the simulated halos, by checking the condition stated in Chapter 2.2.3

$$M_{\text{sub}} > 0.4 M_{*} \text{ and } R_{\text{sub}} = \sqrt{(\mathbf{x}_{\text{sub}} - \mathbf{x}_{\mathbf{C}})^2}$$

with M_{*} being the mass of the Milky Way, $\mathbf{x_{sub}}$ being the position of the subhalo and $\mathbf{x_C}$ being the halo position. I did this for every subhalo of a halo and increasing a variable every time it held true. Unfortunately there is no array generated by the postprocessing that contains the luminosity of subhalos. However I assumed that a galaxy's mass and its luminosity scale almost linear.

Table 3.3: Cluster properties. The values are calculated for > 17000 clusters in total from the maxBCG catalog. Therefore the values are means. Taken from Rykoff et al. 2008.

$\bar{N}_{200}$	9.9	14.0	19.0	22.7	28.6	35.9	44.7	58.4	83.9
$\bar{L}_X$	2.94	6.95	9.05	15.2	24.5	40.3	57.2	86.6	131
$\bar{M}_{200}$	0.41	0.62	0.86	1.07	1.36	1.81	2.02	2.42	4.29

rows: (1) $\bar{N}_{200}$: mean of the used richness range; (2) $\bar{L}_X$: mean x-ray luminosity in $10^{42} h^{-2} erg\ s^{-1}$; (3) $\bar{M}_{200}$: from $\bar{L}_X$ calculated masses according to Equ. 3.7 with the observational parameters $10^{14} M_{\odot}$.

Finally, we can examine the relation between richness and mass in Fig. 3.5. The utilized fitting function was

$$lg\ M_{200} = A(lg\ N_{200} - 1.5) + B, \tag{3.15}$$

resulting in $A = 0.96,\ B = 14.36$ for the observational curve and $A = 1.010, B = 4.10$ for the simulated curve with $\Delta\chi^2 = 12.36$ and $DOF = 1498$. As we can see the normalization is off by a factor ~ 3.5. However, the simulation curve fits the observed clusters from Rykoff et al. 2008 quite well. This may be the result of calculating the masses with the

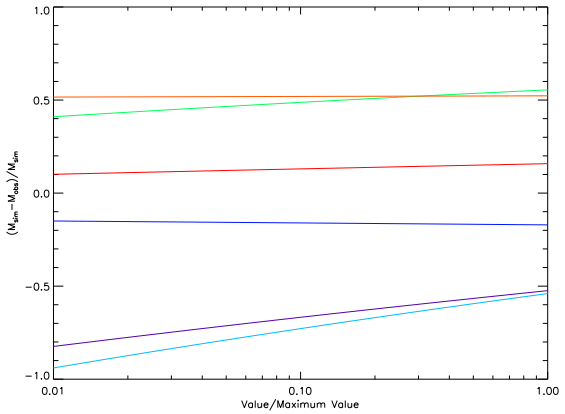

Figure 3.6: Comparison between the residuals of the different mass proxies. The colors represent following scaling relations:
green: temperature - mass
red: luminosity - mass
orange: sze - mass
purple: velocity dispersion - mass
light blue: richness - mass
dark blue: richness - mass calculated from luminosity see Chapter 3.2.5

well approximated luminosity - mass relation shown in Fig. 3.2 and eliminating errors. Furthermore the blue diamonds are just means of the observed clusters. Nevertheless, I fitted the cluster means as well, which resulted in $A = 1.014, B = 4.16$ with $\Delta\chi^2 = 0.005$ and $DOF = 7$. This is an astonishing result. It is important to note that all relations have a slope of ~ 1, which means that for double the richness, the mass is doubled.

3.2.6 Discussion

In Fig. 3.6 a comparison of the residuals of all mass proxies is displayed. They range from approx. 100% too small, to approx. 40% too large. In an astrophysical context these differences are not too big for all scaling relations. We have to keep in mind that scatter plays a big role in fitting. Although the scatter is the smallest for the SZE - mass relation, the residual is compared to the other relations quite big. However, the slope is almost exactly the same. I rank reproducing the slope more important than obtaining the right offset, because the physical behavior rests more in the slope than in the normalization. As we can see, the richness - mass relation falls behind, having the highest offset and a different slope. However the richness - mass relation, fitted to the masses calculated from luminosities, matches the simulation curve almost perfectly with small offset and essentially the same slope. This shows that it is important to keep in mind how the observers obtained the masses they fitted to. If they used masses calculated from SZE it is quite obvious that the relation cannot match if the SZE relation itself does not match. By using the luminosity relation and calculating the masses with a relation that was accurately represented this error is eliminated as seen in the richness scaling relation. Altogether this leads to the conclusion, that richness is well represented in simulations and is a good and easy obtainable mass proxy.

Figure 3.7: Fossilness of galaxy clusters

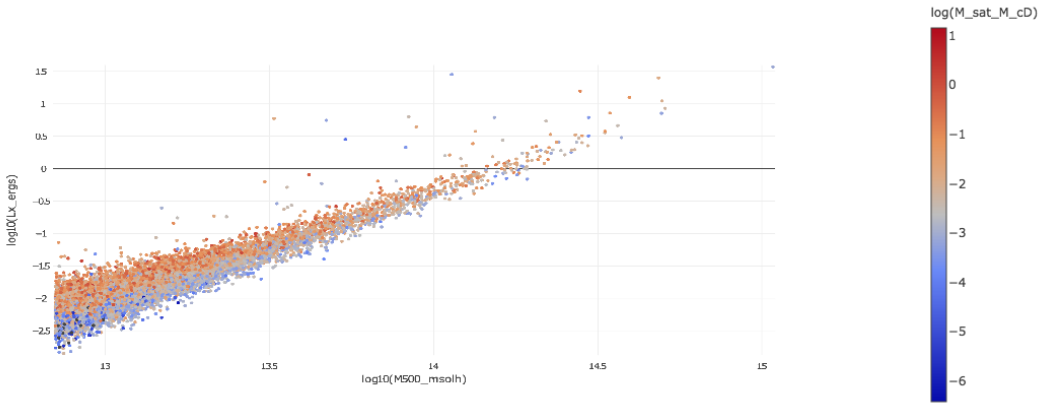

Mass - Luminosity plot of galaxy clusters. The color represents $f = log(M_{cD}/M_{sat})$. Every dot represents a halo from the Magneticum simulation.

3.3 In - Depth look at Luminosity

The on-the-fly post-processing calculates physical properties without taking all hydrodynamical processes into account, to obtain results in short computational times. In this section I want to examine how scaling relations change when second order effects are included. I will restrict myself to the luminosity-mass scaling relation because there are various interesting topics to discuss and doing this for all relations would be repetitive and would simply take too long.

3.3.1 Scatter

The first thing that is immediately visible, looking at Fig. 3.3 is the big scatter. The scatter is a result of dynamical processes like mergers. One way of quantifying it is the so-called fossilness. The study of fossil groups is relatively new (Pratt, Pointecouteau, et al. 2016). N-body simulations of clusters show that galaxy merging naturally produces massive, central galaxies with high surface brightnesses and velocity dispersions. The central galaxy forms through the merger of several massive galaxies along a filament early in the clusters history. If a merger efficient system such as a galaxy group remains undisturbed due to relative isolation from other massive systems, a giant elliptical galaxy will form as a result of the internal multiple merger due to dynamical friction. The time-scale of such a process depends on the local density and is shorter at early epochs. The fraction of mass of the central dominant galaxy to the mass of the most massive satellite is an indicator of how relaxed the system is. Although it is discussed whether fossil groups represent relaxed systems. In Fig. 3.7 the fossilness is color coded. Red colors represent high fossilness, while blue colors represent fractions < 0.3. As can be seen, there is a color gradient along the y-axis, because relaxed systems show less merger activity and are would be less luminous. Therefore a cluster evolves along the scatter similar to stars in the Hertzsprung - Russel diagram. Thus, the scatter can be narrowed by focusing on clusters in a certain stage of relaxation.

Figure 3.8: Fitting maps created with SMAC, depicting one specific galaxy halo. Size of the picture is $4Mpc \times 4Mpc$. *Left panel:* metallicity map *Right panel:* luminosity map

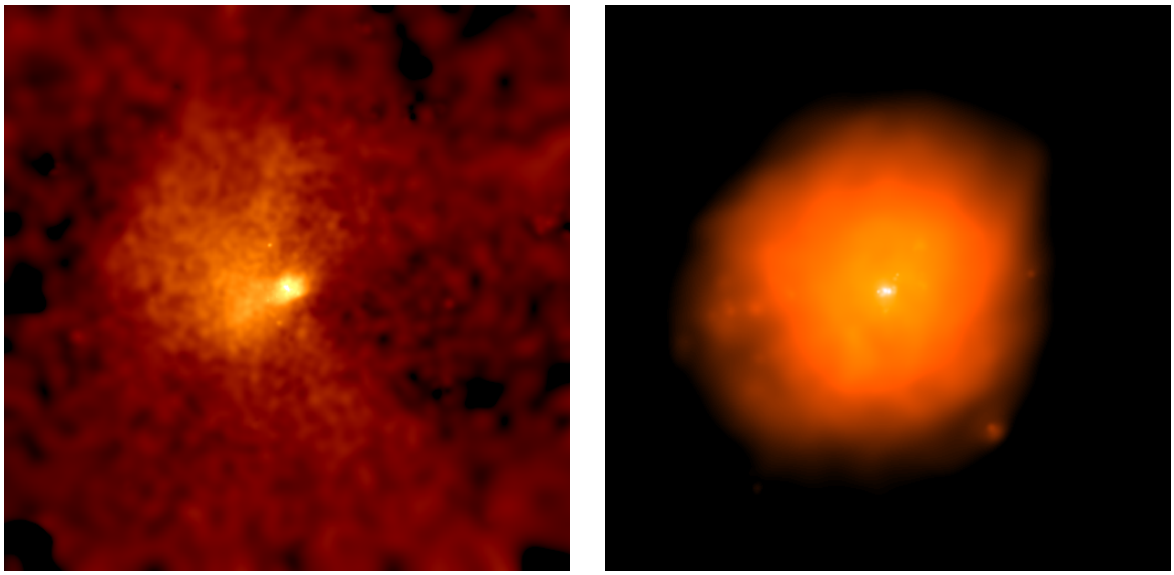

3.3.2 SMAC

The program SMAC is a map making utility for idealized observations. A description of the current implementation of the map making procedure can be found in Dolag et al. 2005. The program returns fit maps with the desired cluster property, taking cooling tables into account. The spectral lines we met in Chapter 2.2.2 are now included in the calculations, increasing the cluster's luminosity and lowering its temperature. Examples for maps created with SMAC can be seen in Fig. 3.8. I created luminosity maps for 874 clusters and calculated their total luminosities. Every pixel contains the value of the luminosity for this region. The total luminosity is obtained by summing up all pixel properties up until the desired radius:

$$L_X = \sum_{r<R_{500}} l_{xy} \, \mathrm{d}A, \tag{3.16}$$

with $\mathrm{d}A = (N_{px}/L)^2 = 512px/4Mpc$. In Fig. 3.9 we can see the comparison between luminosities calculated by the post-processing and by the program SMAC. I fitted both scatters with the same method explained in Chapter 3.2.2., resulting in $A_X = 1.32, B_X = 1.75$ and $\Delta\chi^2 = 9.70$ and $DOF = 26$ for SMAC and $A_X = 1.99, B_X = 1.78$ and $\Delta\chi^2 = 20.26$ and $DOF = 26$ for the post processing. Changes to the post processing fit are due to the fact that I plotted less halos for a better comparison. It is important to note that SMAC generated 54 luminosities, with $L_X < 0.1 \cdot 10^{44} erg\ s^{-1}$ and even five luminosities with $L_X = 0$, while the postprocessing only had five halos with $L_X < 0.1 \cdot 10^{44} erg\ s^{-1}$ and none with $L_X = 0$. As we can see halo luminosities from SMAC tend to be smaller for the same cluster mass. Even though the spectral lines of metals increase the luminosity. The post-processing calculates thermal bremsstrahlung with the temperature and density of the gas, while not distinguishing between intra cluster medium and intra galactic medium. The gas in galaxies is much colder than the ICM, but also much denser. This effect seems to be more dominant than the effect of spectral lines of metals leading to overall higher luminosities calculated by the post-processing. Nevertheless the post-processing is confirmed to be a

Figure 3.9: Comparison between luminosities calculated by SMAC and luminosities calculated by the post-processing. *Left panel:* Every dot represents a MAGNETICUM halo. Red represents SMAC and black represents the post-processing. *Right panel:* Residual plot displaying the weighted difference between the SMAC and the post-processing scaling relation.

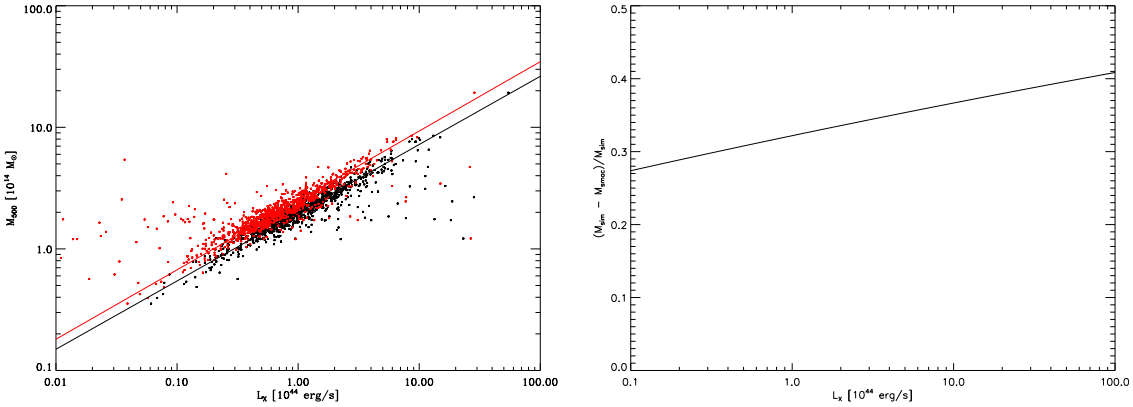

good approximation.

3.3.3 AGN

Another effect, that has an impact on cluster luminosity are AGN. These are neither included in the post-processing nor in SMAC. They have already been discussed in Chapter 2.2.4. To calculate the luminosity of AGN, I first had to check which black hole belongs to which halo

$$\sqrt{(x_{BH} - x_{H,i})^2 + (y_{BH} - y_{H,i})^2 + (z_{BH} - z_{H,i})^2} < R_{vir,i} \tag{3.17}$$

for every black hole. For every found black hole I calculated the three properties

$$L_{\rm bol} = \frac{\epsilon c^2}{1-\epsilon}\dot{M}_{\rm BH},\ \dot{M}_{\rm EDD} = \frac{4\pi G m_p (1-\epsilon)}{\epsilon c \sigma_T} M_{\rm BH},\ L_{\rm EDD} = \frac{4\pi G m_p}{\sigma_T} M_{\rm BH} \tag{3.18}$$

all constants with their normal meaning and $\epsilon = 0.25$. The following equations can be found in Hirschmann et al. 2014. An indicator of how efficient an AGN emits radiation is $f = \dot{L}/\dot{L}_{\rm EDD}$. For high efficiencies I kept the calculated $L_{\rm bol}$ for $f < 0.1$ I calculated it according to

$$\tilde{L}_{bol} = 0.1 L_{\rm EDD}(10\frac{\dot{M}}{\dot{M}_{\rm EDD}})^2 \tag{3.19}$$

Because I am interested in L_X and not $L_{\rm bol}$, I used the third degree polynomial approximation

$$log(L_{\rm HXR}/L_{\rm bol}) = -1.54 - 0.24\mathcal{L} - 0.012\mathcal{L}^2 + 0.0015\mathcal{L}^3$$
$$log(L_{\rm SXR}/L_{\rm bol}) = -1.65 - 0.22\mathcal{L} - 0.012\mathcal{L}^2 + 0.0015\mathcal{L}^3$$

with $\mathcal{L} = log(L_{\rm bol}/L_\odot)$. Furthermore, I only added the sum of both luminosities to the halo luminosity if a random number was smaller than $f_{\rm obsc}$. $f_{\rm obsc}$ represents the probability that a cluster is obscured by surrounding gas. In the left panel of Fig. 3.10 we see the AGN luminosities. It is important to note that only 147 out of 1500 AGN are not obscured. The obscured fraction has a mean of $\bar{f}_{obs} = 0.998$ However there are also four AGNs with $L_X > 200 \times 10^{44}$ erg s^{-1}. The right panel of Fig. 3.10 shows by which factor the fit of halo

Figure 3.10: *Left panel:* luminosities for AGNs in MAGNETICUM halos. *Right panel:* Residual plot displaying the weighted difference between luminosities with and without AGN

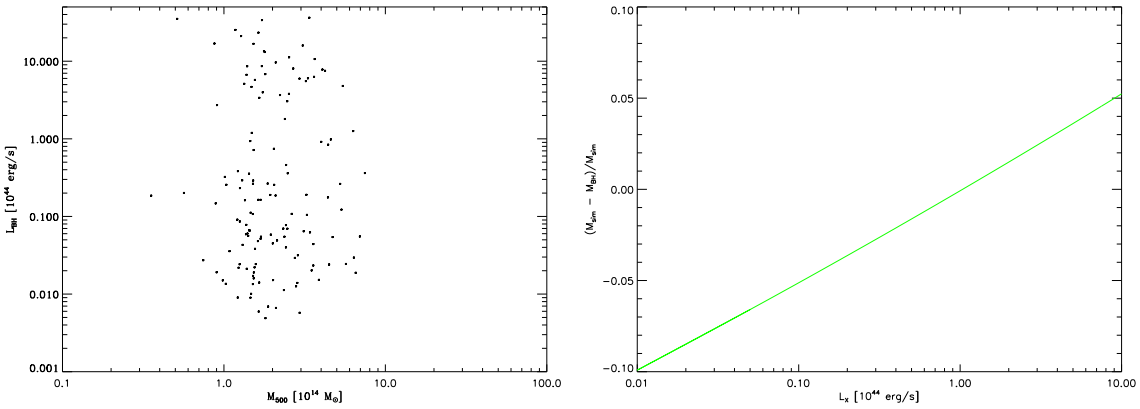

luminosity is increased due to AGN activity. It is calculated with the procedure explained in Chapter 3.2.2, resulting in $A_X = 2.03, B_X = 1.77$ and $\Delta\chi^2 = 41.83$ and $DOF = 27$. We can see that for the lower end AGN increase the luminosity and decrease the luminosity at the higher end. However this is due to the fitting routine, because AGN cannot decrease the luminosity of a halo. With a maximum increase of about 5% the result quite small and the mean increase is even smaller.

Chapter 4

Summary

The study of cluster masses is essential for restraining the cosmological parameters and thus learning about the history and evolution of our universe. While gravitational lensing is a direct way to measure a cluster's mass, it is difficult to obtain and needs background objects in the perfect place. Scaling relations are therefore often the tool of choice. In this thesis I presented the five most prominent ones, being temperature, X-ray luminosity, SZE, velocity dispersion and richness. Richness is a mass proxy that has been sparsely studied in numerical simulations due to its empirical origin. All of these relations vary in various ways. An important factor is the scatter. The SZE has had by far the smallest scatter calculated from the simulation, but also in observations it is popular for its small scatter. Merger activity is a main cause of scatter, represented by the fossilness plot. Furthermore the slope of the SZE relation fits perfectly, although there is a comparatively large offset. The offsets in the scaling relations may be due to the fact that observers use masses that are calculated by an effect that is not well represented. By comparing luminosities calculated from SMAC and post-processing, we saw that there can be a difference of up to 40% by taking more hydrodynamical effects into account. This is one reason why there are partly larger offsets. AGN activity seems to have insignificant impact, at least on halo luminosity. The SZE is a very small effect and therefore not easy and cheap to measure for large samples of clusters. In comparison richness is just that. Although falling behind to the other relations in a first approach, it matched well by nesting it in a richness - luminosity relation. That richness is represented by numerical simulations at all is not obvious. I come to the result, that richness is well represented in the Magneticum simulation, allowing a better comparison to observational data.

Acknowledgements

An dieser Stelle möchte ich mich bei allen Personen bedanken, die mich im Laufe meiner Bachelorarbeit unterstützt und motiviert haben. Inbesondere gilt dieser Dank meinem Betreuer Klaus Dolag. Er hat sich stets die Zeit genommen mir bei meinen Problemen zu helfen und hat mich immer wieder bei meiner Recherche unterstützt. Desweiteren bin sehr dankbar, dass ich hier an der Sternwarte meine Bachelorarbeit schreiben konnte. Von den Masteranden, Doktoranden und vorallem Rhea-Silvia Remus, bei ihr möchte ich mich hiermit auch für die Korrektur meiner Arbeit bedanken, wurde eine Atmosphäre geschaffen, wegen derer ich jeden Tag mit Freude an die Sternwarte gekommen bin. Nicht nur, weil jede/r einzelne/r mir wie selbstverständlich bei meinen Fragen weitergeholfen hat, sondern auch durch die interessanten, fachfremden Diskussionen.

Bibliography

Abell, G. O. (1958). "The Distribution of Rich Clusters of Galaxies." In: 3, p. 211. DOI: 10.1086/190036.

Andreon, S. and M. A. Hurn (2010). "The scaling relation between richness and mass of galaxy clusters: a Bayesian approach". In: 404, pp. 1922–1937. DOI: 10.1111/j.1365-2966.2010.16406.x. arXiv: 1001.4639.

Bocquet, S. et al. (2014). "Mass Calibration and Cosmological Analysis of the SPT-SZ Galaxy Cluster Sample Using Velocity Dispersion and X-ray Measurements". In: DOI: 10.1088/0004-637X/799/2/214. eprint: arXiv:1407.2942.

Böhringer, H., K. Dolag, and G. Chon (2012). "Modelling self-similar appearance of galaxy clusters in X-rays". In: 539, A120, A120. DOI: 10.1051/0004-6361/201118000. arXiv: 1112.5035.

Croton, D. (2013). "Damn You, Little h! (Or, Real-World Applications of the Hubble Constant Using Observed and Simulated Data)". In: 30, e052, e052. DOI: 10.1017/pasa.2013.31. arXiv: 1308.4150.

Dolag, K. et al. (2005). "The imprints of local superclusters on the Sunyaev-Zel'dovich signals and their detectability with Planck". In: 363, pp. 29–39. DOI: 10.1111/j.1365-2966.2005.09452.x. eprint: astro-ph/0505258.

Garrett, Katherine and Gintaras Duda (2010). "Dark Matter: A Primer". In: DOI: 10.1155/2011/968283. eprint: arXiv:1006.2483.

Henry, P. and W. Tucker (1979). "A luminosity-temperature relation for cluster X-ray sources". In: 229, pp. 78–82. DOI: 10.1086/156931.

Hirschmann, M. et al. (2014). "Cosmological simulations of black hole growth: AGN luminosities and downsizing". In: 442, pp. 2304–2324. DOI: 10.1093/mnras/stu1023. arXiv: 1308.0333.

Ilić, S., A. Blanchard, and M. Douspis (2015). "X-ray galaxy clusters abundance and mass temperature scaling". In: 582, A79, A79. DOI: 10.1051/0004-6361/201526793. arXiv: 1510.02518.

Komatsu, E. et al. (2010). "Seven-Year Wilkinson Microwave Anisotropy Probe (WMAP) Observations: Cosmological Interpretation". In: DOI: 10.1088/0067-0049/192/2/18. eprint: arXiv:1001.4538.

Kravtsov, A. V., A. Vikhlinin, and D. Nagai (2006). "A New Robust Low-Scatter X-Ray Mass Indicator for Clusters of Galaxies". In: 650, pp. 128–136. DOI: 10.1086/506319. eprint: astro-ph/0603205.

Magorrian, J. et al. (1998). "The Demography of Massive Dark Objects in Galaxy Centers". In: 115, pp. 2285–2305. DOI: 10.1086/300353. eprint: astro-ph/9708072.

Padovani, P. (1997). "Unified schemes for radio-loud AGNs: recent results". In: 68, p. 47. eprint: astro-ph/9701074.

Pratt, G. W., J. H. Croston, et al. (2009). "Galaxy cluster X-ray luminosity scaling relations from a representative local sample (REXCESS)". In: 498, pp. 361–378. DOI: 10.1051/0004-6361/200810994. arXiv: 0809.3784.

Pratt, G. W., E. Pointecouteau, et al. (2016). "The hot gas content of fossil galaxy clusters". In: DOI: 10.1051/0004-6361/201628462. eprint: arXiv:1604.08223.

Ruel, J. et al. (2014). "Optical Spectroscopy and Velocity Dispersions of Galaxy Clusters from the SPT-SZ Survey". In: 792, 45, p. 45. DOI: 10.1088/0004-637X/792/1/45. arXiv: 1311.4953.

Rykoff, E. S. et al. (2008). "Measuring the Mean and Scatter of the X-Ray Luminosity-Optical Richness Relation for maxBCG Galaxy Clusters". In: 675, 1106-1124, pp. 1106–1124. DOI: 10.1086/527537. arXiv: 0709.1158.

Salpeter, E. E. (1964). "Accretion of Interstellar Matter by Massive Objects." In: 140, pp. 796–800. DOI: 10.1086/147973.

Schneider, P. (2015). *Extragalactic Astronomy and Cosmology: An Introduction*. DOI: 10.1007/978-3-642-54083-7.

Springel, V. (2005). "The cosmological simulation code GADGET-2". In: 364, pp. 1105–1134. DOI: 10.1111/j.1365-2966.2005.09655.x. eprint: astro-ph/0505010.

Wolf, M. (1901). "Ein merkwürdiger Haufen von Nebelflecken". In: *Astronomische Nachrichten* 155, p. 127. DOI: 10.1002/asna.19011550608.

Selbstständigkeitserklärung

Hiermit erkläre ich, dass ich die vorliegende Arbeit eigenständig und ohne fremde Hilfe angefertigt habe. Textpassagen, die wörtlich oder dem Sinn nach auf Publikationen oder Vorträgen anderer Autoren beruhen, sind als solche kenntlich gemacht. Die Arbeit wurde bisher keiner anderen Prüfungsbehörde vorgelegt und auch noch nicht veröffentlicht.

München, 31.07.2017
Ort, Datum

Unterzeichner